Cell

PKCε Promotes Oncogenic Functions of ATF2 in the Nucleus while Blocking Its Apoptotic Function at Mitochondria

Eric Lau,[1] Harriet Kluger,[2] Tal Varsano,[1] KiYoung Lee,[3,5] Immo Scheffler,[4] David L. Rimm,[2] Trey Ideker,[3] and Ze'ev A. Ronai[1,*]
[1]Signal Transduction Program, Sanford-Burnham Medical Research Institute, La Jolla, CA 92037, USA
[2]Department of Pathology, Yale University, New Haven, CT 06520, USA
[3]Departments of Medicine and Bioengineering
[4]Department of Biology
University of California, San Diego, La Jolla, CA 92093 USA
[5]Department of Biomedical Informatics, Ajou University School of Medicine, Suwon 443-749, Korea
*Correspondence: ronai@sbmri.org
DOI 10.1016/j.cell.2012.01.016

SUMMARY

The transcription factor ATF2 elicits oncogenic activities in melanoma and tumor suppressor activities in nonmalignant skin cancer. Here, we identify that ATF2 tumor suppressor function is determined by its ability to localize at the mitochondria, where it alters membrane permeability following genotoxic stress. The ability of ATF2 to reach the mitochondria is determined by PKCε, which directs ATF2 nuclear localization. Genotoxic stress attenuates PKCε effect on ATF2; enables ATF2 nuclear export and localization at the mitochondria, where it perturbs the HK1-VDAC1 complex; increases mitochondrial permeability; and promotes apoptosis. Significantly, high levels of PKCε, as seen in melanoma cells, block ATF2 nuclear export and function at the mitochondria, thereby attenuating apoptosis following exposure to genotoxic stress. In melanoma tumor samples, high PKCε levels associate with poor prognosis. Overall, our findings provide the framework for understanding how subcellular localization enables ATF2 oncogenic or tumor suppressor functions.

INTRODUCTION

Activating transcription factor 2 (ATF2) is one of 16 Atf/Creb family transcription factors and an integral component of the activator protein-1 (AP-1) transcriptional complex, which regulates normal cellular growth and development, as well as cellular response to stress (Lopez-Bergami et al., 2010). The diverse transcriptional functions of ATF2 are attributed to its homo- or heterodimerization with other AP-1 transcription factors via a basic leucine zipper (bZIP) domain, in concert with its phosphorylation by stress kinases, JNK or p38, on residues 69/71 (Gupta et al., 1995). As a stress-inducible transcription factor, ATF2 regulates gene expression programs implicated in cell-cycle control, cytokine expression, and cell death (Lopez-Bergami et al., 2010). In addition to its transcriptional role, ATF2 functions in the DNA damage response, which requires ATM-dependent phosphorylation on residues 490/498. Mice harboring mutations at these sites are more radiosensitive and genetically unstable when crossed with p53 mutant mice or when subjected to a skin carcinogenesis protocol (Bhoumik et al., 2005; Li et al., 2010).

Though the above functions require nuclear localization, growing evidence points to cytoplasmic localization of ATF2, although its function there remains elusive. In melanomas, nuclear ATF2 is associated with metastasis and poor prognosis, whereas cytoplasmic ATF2 is associated with nonmalignant skin cancers and better prognosis (Berger et al., 2003). ATF2 transcriptional activity (which requires nuclear localization) is required for melanoma development, as demonstrated in the N-Ras/Ink4a mouse melanoma model (Shah et al., 2010). Correspondingly, inhibition of ATF2 nuclear localization by expression of either 10 or 50 amino acid (aa) peptides derived from ATF2 efficiently attenuates melanoma development (Bhoumik et al., 2004). In contrast, ATF2 cytosolic localization, as seen in nonmalignant skin cancer, is associated with a tumor suppressor role; inhibiting ATF2 in keratinocytes results in a greater number of skin papillomas that develop more rapidly than WT ATF2-expressing keratinocytes (Bhoumik et al., 2008).

We investigated mechanisms underlying the ability of ATF2 to elicit diverse nuclear and cytoplasmic functions and report that ATF2 functions at the mitochondria in response to genotoxic stress. We found that, at the mitochondrial outer membrane, ATF2 abrogates formation of high-order complexes containing hexokinase-1 (HK1) and voltage-dependent anion channel-1 (VDAC1), deregulating mitochondrial outer-membrane permeability and initiating apoptosis. This function is negatively regulated by PKCε phosphorylation of ATF2, which dictates its nuclear localization. Of note, elevated expression and activity of PKCε was reported in different tumor types and is associated with poorer outcome and inhibition of tumor cell

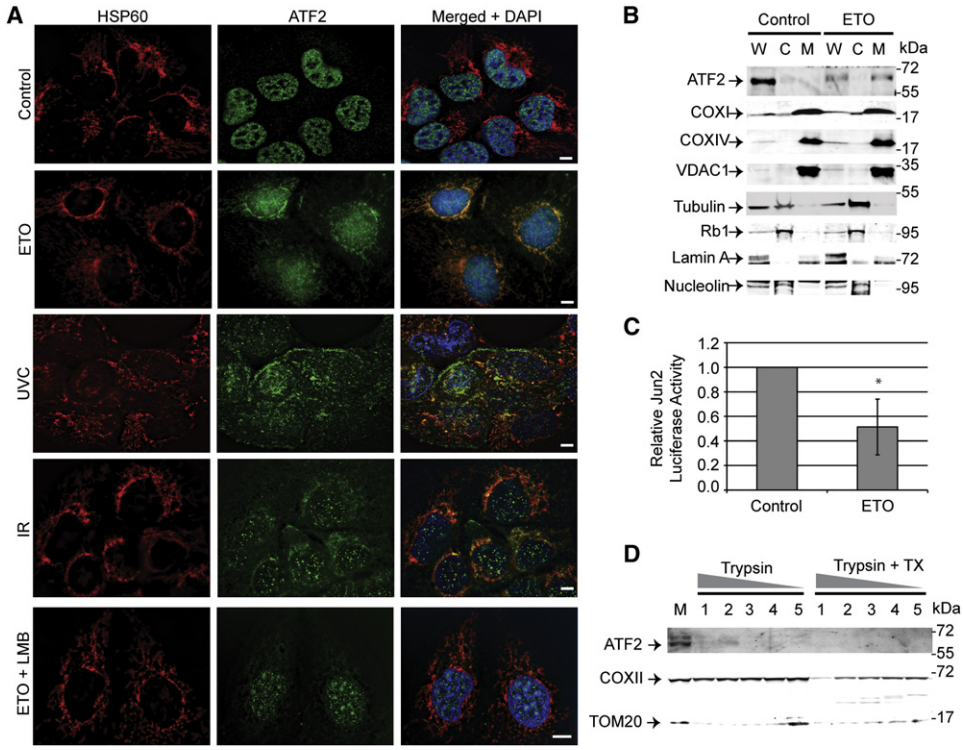

Figure 1. ATF2 Localizes at the Mitochondrial Outer Membrane in Response to Genotoxic Stress

(A) Control, 5 μM etoposide-treated (ETO, overnight treatment), UVC-treated (20 J/m^2), ionizing radiation-treated (IR, 5Gy), or 40 ng/ml leptomycin B (LMB) and ETO cotreated SCC9 cells grown on coverslips were immunofluorescently stained for HSP60 (red), ATF2 (green), or DNA (blue). Control and ETO panels represent 89% ± 4% and 64% ± 11%, respectively, of the cells from three independent replicate coverslips per condition. n > 100 cells counted per replicate.

(B) Control- or ETO-treated SCC9 cells were harvested for whole-cell lysate (W) or biochemically fractionated to cytoplasmic (C) and mitochondrial (M) fractions and were subject to immunoblot analysis with indicated antibodies.

(C) Jun2 promoter-luciferase-transfected SCC9 cells were assayed for luciferase activity prior to (Control) or after ETO treatment. *p < 0.0001.

(D) Mitochondria (M) purified from ETO-treated SCC9 cells were subject to proteolysis protection assay with titrated concentrations of trypsin: 0.2 (1), 0.1 (2), 0.05 (3), 0.025 (4), or 0.0125 (5) μg in the absence or presence of 1% Triton X-100 (TX) detergent.

Scale bars, 10 μm. Error bars represent SD. See also Figure S1.

death (Bae et al., 2007). Whereas PKCε overexpression promotes the development of squamous carcinomas (Sand et al., 2010), its inhibition sensitizes tumor cells to cell death (Gillespie et al., 2005). The identification of mechanisms underlying ATF2 subcellular localization and cytosolic function offers a framework for understanding the regulation of opposing functions for the same transcription factor.

RESULTS

Genotoxic Stress Induces ATF2 Nuclear Export and Mitochondrial Localization

Although ATF2 cytoplasmic localization was previously reported (Berger et al., 2003; Bhoumik et al., 2008; Deng et al., 2008), a cytoplasmic function has yet to be described. Based on the observed cytosolic localization of ATF2 in squamous cell carcinoma (SCC) tumors, we employed a SCC line (SCC9) to analyze potential ATF2 cytoplasmic function. Mass spectrometric (MS) analysis of cytosol-localized ATF2-bound proteins in SCC9 cells identified a cluster of mitochondria-outer membrane-related proteins, suggesting an ATF2 mitochondrial interaction (Table S1 available online). Indeed, nonstressed SCC9 cells exhibit predominantly nuclear ATF2, whereas genotoxic stress rendered by etoposide (ETO) resulted in its accumulation at mitochondria in ~64% of treated cells (Figure 1A). Other genotoxic insults, including ultraviolet C (UVC, 20 J/m^2) and ionizing irradiation (IR, 5Gy), also prompted the mitochondrial localization of ATF2 (Figure 1A). The mitochondrial localization of ATF2 following genotoxic stimuli was also seen in other cell types, including normal human fibroblasts (HSF), primary human keratinocytes (NHEK), and melanocytes (HEM), as well as in other SCC cell lines (M7 and P9) (Figure S1). Of note, whereas some melanoma cell lines (UACC903) exhibit partial mitochondrial enrichment of ATF2 (Figures S1 and 6D), a number of melanoma cell lines (LU1205 and 501Mel) (Figures S1 and 6D) did not exhibit mitochondrial localization of ATF2 following genotoxic stimuli, with the exception of IR (Figure S1), suggesting that malignant melanomas are largely resistant to genotoxic stress-induced mitochondrial translocation of ATF2. The extent of ATF2 mitochondrial localization differs among the different cultures and type of stimuli, indicating variation in cellular response and control of such translocation

in each of these cultures. Biochemical fractionation of SCC9 cells confirmed that exposure to genotoxic stress results in the accumulation of ATF2 in mitochondrial-enriched fractions (Figure 1B).

Pretreatment of SCC9 cells with the nuclear export inhibitor leptomycin B (LMB) prevented mitochondrial accumulation of ATF2 following ETO treatment, indicating that nuclear export of ATF2 occurs after genotoxic stress (Figure 1A, fifth row). Consistently, we observed an ~50% reduction of luciferase activity driven by the ATF2 response element (Figure 1C).

ATF2 protein does not harbor canonical mitochondrial localization or peptide-processing signals, which could facilitate import or insertion into mitochondrial membranes, suggesting that its mitochondrial localization requires interaction with mitochondrial protein(s). Thus, we examined where ATF2 might be accumulating at the mitochondrial outer membrane (MOM), the intermembrane space (IMS), the mitochondrial inner membrane (MIM), or the mitochondrial inner matrix. Limited proteolysis protection assays with enriched mitochondrial fractions purified from ETO-treated SCC9 cells revealed efficient degradation of ATF2 in the absence of detergent, consistent with the degradation pattern of the MOM component TOM20 but differing from the pattern of inner-matrix protein COXII, which is degraded only in the presence of detergent (Figure 1D). These results suggest that, in response to genotoxic stress, ATF2 localizes at the MOM.

ATF2 Interacts with HK1:VDAC1 Complexes following Genotoxic Stress

To determine ATF2 function at mitochondria, we tested MOM protein(s) identified in our MS analysis (Table S1), hexokinase-1 (HK1) and voltage-dependent anion channel 1 (VDAC1) (Figure S1), for possible interaction with ATF2.

In response to various forms of stress, HK1 and HK2 bind to VDAC1, which oligomerizes to form large molecular weight complexes (Abu-Hamad et al., 2009). To determine whether ATF2 is part of these complexes, we assessed the distribution of ATF2, HK1, and VDAC1 in fractions obtained following fast protein liquid chromatographic (FPLC) analysis using a gel filtration column. Whereas prior to stress, ATF2 did not codistribute to fractions with HK1 and VDAC1, after ETO treatment, all three proteins were found within high molecular weight fractions (Figure 2A). Of note, not all of the ATF2 protein redistributed to high MW fractions. The remaining ATF2 in the low MW fraction is consistent with the residual nuclear ATF2 found by IHC and the residual (~50%) transcriptional activity recorded after ETO treatment (Figures 1A and 1C, respectively). As shown below, distinct posttranslational modification of ATF2 is found in these pools.

To confirm the interaction of ATF2 with HK1 and VDAC1, we immunoprecipitated endogenous ATF2 or HK1 from cell lysates of SCC9 cells prior to and after ETO treatment. ATF2 interaction with HK1 and with high molecular weight (~130 kDa) tetrameric VDAC1 oligomers, detectable with the aid of crosslinker (Zalk et al., 2005), was clearly seen after ETO treatment (Figure 2B, top and bottom). Interestingly, knockdown of HK1, but not HK2, abrogated mitochondrial localization of ATF2 following ETO treatment, indicating that the mitochondrial localization of ATF2 requires HK1 (Figures 2C, 2D, and S2A).

PKCε Phosphorylation Negatively Regulates ATF2 Mitochondrial Localization

Phosphorylation of ATF2 by p38 or JNK on Thr69/71 is required for its dimerization with AP-1 transcription factors and for transcriptional activity (Gupta et al., 1995; van Dam et al., 1995). However, Thr69/71 phosphorylation was dispensable for ATF2 mitochondrial localization, as inhibition of either p38 or JNK activity by respective pharmacological inhibitors did not alter its nuclear localization (Figure S2B).

Analysis of ATF2 protein sequence using the phosphorylation site scanning program (http://scansite.mit.edu) predicted an uncharacterized but highly probable PKCε/δ/ζ phosphorylation site on residue Thr52. Treatment with the PKCε translocation inhibitor (PKCε-i) promoted mitochondrial localization of ATF2, even in the absence of ETO, as detected by both IHC and mitochondrial fractionation (Figures 3A and S3F). Consistently, siRNA-mediated knockdown of PKCε (Figure S3A) promoted mitochondrial localization of ATF2 (Figure 3B), whereas overexpression of a constitutively active form of PKCε (caPKCε; Pass et al., 2001) attenuated ATF2 accumulation at mitochondria following ETO treatment (Figure 3C). As with the genotoxic stress-induced nuclear export of ATF2 (Figure 1A), LMB pretreatment blocked its mitochondrial translocation following PKCε inhibition (Figure S3E). Inhibition of the novel (δ) or atypical (ζ) PKC forms had negligible effect on mitochondrial ATF2 localization (Figure S3B). These observations indicate that ATF2 mitochondrial localization is primarily regulated by PKCε. Of note, Ser729 phosphorylation on PKCε, an indicator of active PKCε, decreases following overnight treatment with ETO or with PKCε-i (Figure 3D), suggesting that the effect of PKCε on the nuclear localization of ATF2 is attenuated following genotoxic stress, enabling ATF2 nuclear export and mitochondrial localization.

To determine whether the predicted ATF2 site (Thr52) for phosphorylation by PKCε regulates mitochondrial translocation of ATF2, we assessed PKCε phosphorylation of ATF2 in vitro, as well as the localization of $ATF2^{T52A}$ (a nonphosphorylatable alanine phosphomutant) and $ATF2^{T52E}$ (a glutamic acid phosphomimic). In vitro kinase assays employing an ATF2 fragment consisting of aa 50–100 revealed that PKCε phosphorylates the wild-type (WT), but not the $ATF2^{T52A}$, peptide. Addition of PKC catalytic inhibitor Gö6850 inhibited this phosphorylation (Figure 3E). Together, these data indicate that Thr52 is a PKCε phosphoacceptor site. Consistent with the nuclear localization observed in the presence of caPKCε, the $ATF2^{T52E}$ mutant exhibited constitutive nuclear localization (Figure 3F), whereas the $ATF2^{T52A}$ mutant localized to the cytoplasm and mitochondria, even in the absence of genotoxic stress (Figure 3F). Gel filtration analysis revealed that $ATF2^{T52A}$, but not $ATF2^{T52E}$, distributed to large molecular weight fractions containing VDAC1 (Figure S3D). Interestingly, expression of $ATF2^{T52A}$ revealed less HK1 within the high molecular weight VDAC1-containing fractions, pointing to the possibility that $ATF2^{T52A}$ may attenuate the interaction between HK1 and VDAC1.

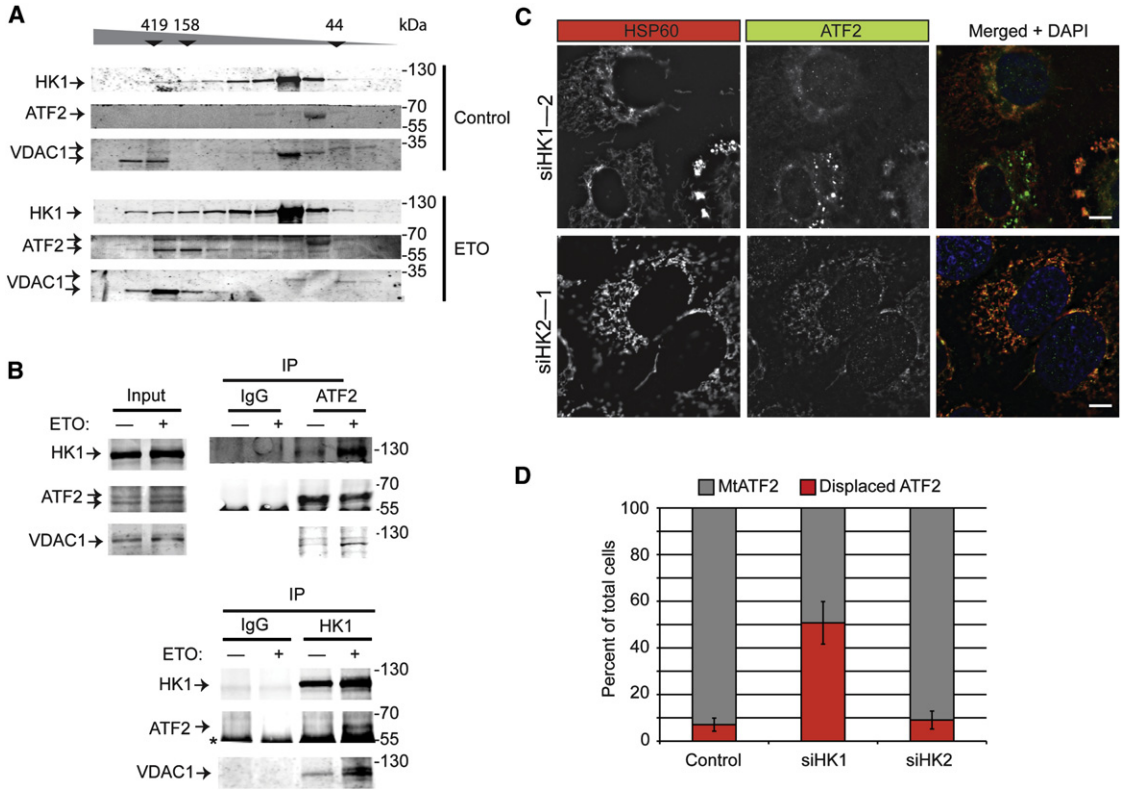

Figure 2. ATF2 Interacts with VDAC1 and HK1 Complex at the Mitochondria

(A) Control or 5 μM etoposide (ETO, overnight)-treated SCC9 cells were lysed and subject to size exclusion chromatography separation. Every other fraction was subject to immunoblot analysis with indicated antibodies. Fractions are arranged, left to right, in order of descending molecular weight, with control protein weight markers indicated above (in kDa).

(B) Control- or ETO-treated SCC9 cells were crosslinked and lysed. ATF2 (top) or HK1 (bottom) were immunoprecipitated and subject to immunoblot analysis with indicated antibodies. Asterisk indicates nonspecific IgG.

(C) Coverslip-grown SCC9 cells knocked down for either HK1 or HK2 and subject to ETO treatment were immunofluorescently stained with indicated antibodies.

(D) Quantitation of mitochondrial ATF2 (MtATF2, gray bars) versus displaced ATF2 (red bars) before or after knockdown of HK1 or HK2. n > 50 cells per replica in three independent experiments.

Scale bars, 10 μm. Error bars represent SD. See also Figure S2 and Table S1.

Collectively, these findings establish that PKCε regulates ATF2 mitochondrial localization via phosphorylation at T52.

Given the effect of PKCε on ATF2 subcellular localization, we next assessed its effect on ATF2 transcriptional activity. Overexpression of caPKCε led to a marked increase in Jun2-luciferase activity, indicative of ATF2 transcriptional activity, which was largely attenuated upon knockdown of ATF2 (Figure 3G). Interestingly, inhibition with Gö6850 or ETO treatment reduced Jun2-luciferase activity to similar extents as knockdown of ATF2, suggesting that PKCε contributes to basal transcriptional activity of ATF2 in these cells. Consistently, reconstitution of SCC9 cells carrying a stable knockdown of ATF2 (employing shRNA targeting ATF2 3′UTR) (Figure S3C) with $ATF2^{T52E}$ also increased Jun2-luciferase activity compared to $ATF2^{WT}$. Conversely, mutation of T52 to alanine abolished ATF2 transcriptional activity (Figure 3H). These findings indicate that, by regulating ATF2 nuclear localization, PKCε not only determines ability of ATF2 to reach the mitochondria, but also its transcriptional activity.

Mitochondria-Localized ATF2 Compromises Outer Membrane Integrity by Disrupting HK1:VDAC1 Complexes

Disruption of VDAC interaction with HK1 or HK2 sensitizes cells to stress, promoting MOM leakage of molecules from the IMS (Abu-Hamad et al., 2009). Conversely, HK1 or HK2 binding to the MOM promotes resistance to stress and increased cell survival (Moin et al., 2007; Shoshan-Barmatz et al., 2010; Shulga et al., 2009). To assess whether interaction with ATF2 perturbs the HK1/VDAC1 complex, we first evaluated HK1 accumulation at mitochondria following ectopic expression of the ATF2 phosphomutants that preferentially localize to either the nucleus ($ATF2^{T52E}$) or mitochondria ($ATF2^{T52A}$) (Figures 4 and S4D). Under basal conditions, HK1 is localized to the cytoplasm and mitochondria (Figure 4A). Of note, mitochondrial colocalization of HK1 was enhanced after ETO treatment (Figure 4B). In $ATF2^{T52E}$-transfected cells, HK1 accumulation at mitochondria was similar to that seen in control cells prior to and after ETO treatment (Figures 4G and 4H). However, $ATF2^{T52A}$

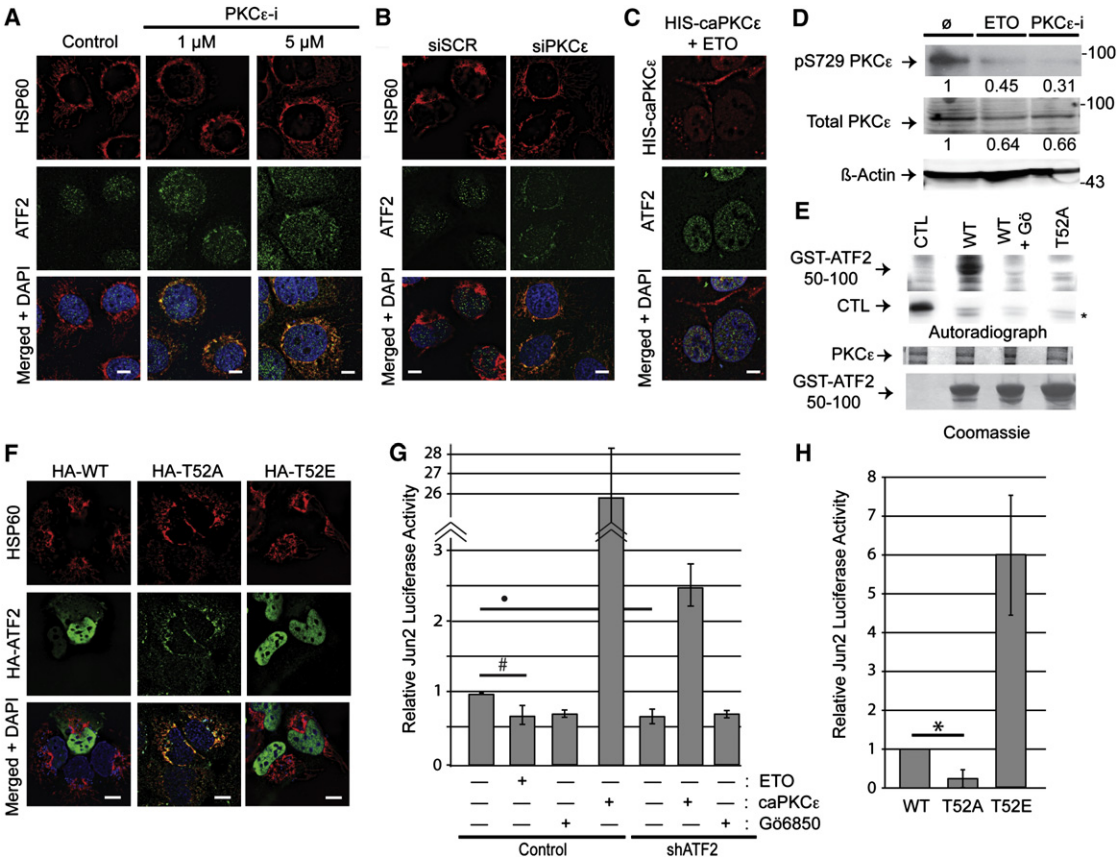

Figure 3. PKCε Phosphorylation of ATF2 on Thr52 Negatively Regulates Its Mitochondrial Localization

(A–C) Coverslip-grown SCC9 cells were immunofluorescently stained with indicated antibodies after: (A) overnight treatment with 1 or 5 μM PKCε translocation inhibitor (PKCε-i); (B) overnight treatment with 20 nM scrambled control (siSCR) or PKCε-targeted (siPKCε) siRNA; and (C) transfection with HIS-tagged constitutively active PKCε (caPKCε, red) and treatment with 5 μM etoposide (ETO, overnight).

(D) SCC9 cells treated overnight with ETO or 5 μM PKCε translocation inhibitor (PKCε-i) were lysed and subject to immunoblot analysis with indicated antibodies.

(E) In vitro PKCε kinase assay with Millipore control peptide (CTL), purified GST-ATF2 50–100 aa WT (WT), GST-ATF2 50–100 aa WT + PKCε catalytic inhibitor, Gö6850 (WT+Gö), or GST-ATF2 50–100 aa T52A (T52A) as substrate. *nonspecific bands. Coomassie-stained gel (bottom) and autoradiograph (top) are displayed as indicated.

(F) Coverslip-grown SCC9 cells were transfected with HA-tagged wild-type ATF2 (WT), ATF2^{T52A}, or ATF2^{T52E} and were subsequently immunofluorescently stained with indicated antibodies.

(G) SCC9 control or ATF2 knocked down cells (shATF2) were transfected with Jun2 promoter-luciferase construct, and either empty vector (EV) or caPKCε were assayed for luciferase activity before and after overnight ETO or Gö6850 (2 μM) treatment. •p = 0.0034; #p = 0.0157.

(H) SCC9 cells stably knocked down for ATF2 with a 3′UTR-targeted shRNA were reconstituted with Jun2 promoter-luciferase construct and ATF2^{WT}, ATF2^{T52A}, or ATF2^{T52E} and were subsequently assayed for luciferase activity. *p = 0.0047.

Scale bars, 10 μm. Error bars represent SD. See also Figure S3.

overexpression abrogated mitochondrial accumulation of HK1 prior to and following genotoxic stress, as indicated by decreased distinct colocalization of HK1 and MitoTracker (Figures 4E and 4F and insets 4E* and 4F*). Of note, ETO-treated, ATF^{T52A}-expressing cells exhibited more fragmented mitochondria compared to cells expressing empty vector, ATF2^{WT}, or ATF2^{T52E} (Figure insets 4E* and 4F*, compared to Figures 4A–4C, 4G, and 4H). Further, the expression of ATF2^{T52A} promoted the appearance of punctated, HK1 positively staining structures that localized near, but not with, the MitoTracker-labeled mitochondrial structures (Figures 4E and 4F and insets E* and F* and Figure S4E). These results indicate that mitochondrial translocation of ATF2 perturbs HK1/VDAC1 complexes and MOM integrity. ATF2^{WT} also translocated to the mitochondria and abrogated HK1 localization following genotoxic stress (Figure 4D). Expression of either ATF2^{WT} or the T52 ATF2 mutants did not affect VDAC1 multimerization, a change that promotes mitochondrial leakage and cell death, as assessed by crosslinking and nonreducing immunoblot analysis (data not shown).

Consistent with our IHC data, overexpression of ATF2^{T52A} abrogated HK1 association with VDAC1 that was immunoprecipitated under basal conditions and following genotoxic stress. Overexpression of ATF2^{WT} abrogated the HK1/VDAC1 complex only after ETO treatment, whereas the ATF2^{T52E} did not affect HK1 binding to VDAC1 (Figure 5A). In agreement, HK1 association with VDAC1 also decreased following treatment of SCC9

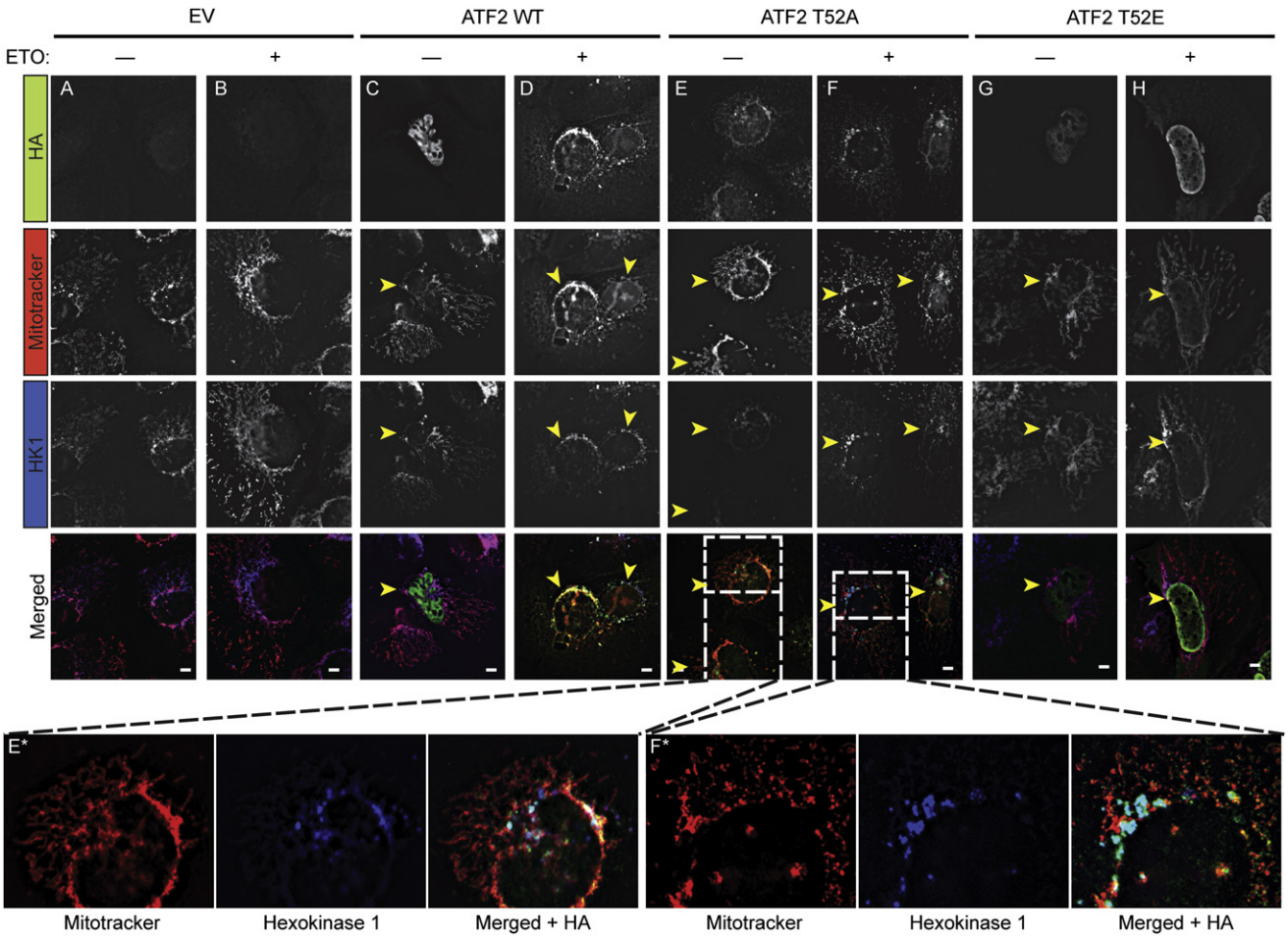

Figure 4. ATF2^{T52A} Displaces HK1 from Mitochondria

(A–H) Coverslip-grown SCC9 cells were transfected with empty vector (EV) or HA-tagged ATF2 (WT), ATF2^{T52A}, or ATF2^{T52E} in the absence (A, C, E, E*, G) or presence (B, D, F, F*, H) of 5 μM etoposide (ETO, overnight) and were subsequently immunostained with indicated antibodies and MitoTracker. Yellow arrowheads indicate HA-positive cells. Scale bars, 10 μm. See also Figure S4.

cells with PKCε-i alone or PKCε-i in the presence of ETO (Figure 5B). These data indicate that mitochondria-localized ATF2 attenuates the ability of HK1 to form a complex with VDAC.

ATF2 Localization at the Mitochondria Reduces Mitochondrial Potential and Sensitizes Cells to Genotoxic Stress-Induced Death

We next monitored changes in mitochondrial membrane potential that are reflective of leakage. We used fluorescence-activated cell sorting (FACS) to quantify tetramethylrhodamine ethyl ester (TMRE) uptake, an indicator of relative mitochondrial membrane potential. Consistent with previous reports (Fu et al., 2008), low-dose ETO initially increased TMRE uptake by control SCC9 cells (Figure S4A), whereas increased doses of ETO reduced TMRE uptake (data not shown).

ATF2^{T52E}-transfected SCC9 cells did not exhibit altered TMRE uptake compared to empty vector- (EV) or ATF2^{WT}-transfected cells. These, as well as EV-transfected cells, increased TMRE uptake following genotoxic stress (Figure S4A). In contrast, ATF2^{T52A}-transfected cells decreased TMRE uptake (Figures S4A and S4C), consistent with our IHC data, indicating that mitochondrial ATF2 impairs the formation of HK1/VDAC1 complexes and thus MOM integrity.

As changes in the absolute number of mitochondria (mitochondrial mass) need to be monitored in order to determine net changes in mitochondrial potential, we pulse labeled SCC9 cells with nonyl-acridine orange (NaO) to stain for cardiolipin, a mitochondrial lipid that is unaffected by altered membrane potential. ATF2^{T52A}-expressing, but not ATF2^{T52E}-expressing, cells increased NaO staining, indicating that loss of mitochondrial membrane potential increased mitochondrial biogenesis, likely to compensate for dysfunctional mitochondria (Figures S4B and S4C), consistent with previous reports (Fu et al., 2008). Of note, the observed TMRE/NaO ratios, reflective of membrane potential per mitochondria (mitochondrial "leakiness"), indicate that overexpression of ATF2^{T52A}, but not of ATF2^{WT} or ATF2^{T52E}, decreases membrane potential relative to control cells (Figures 5C). Correspondingly, only ATF2^{T52A}

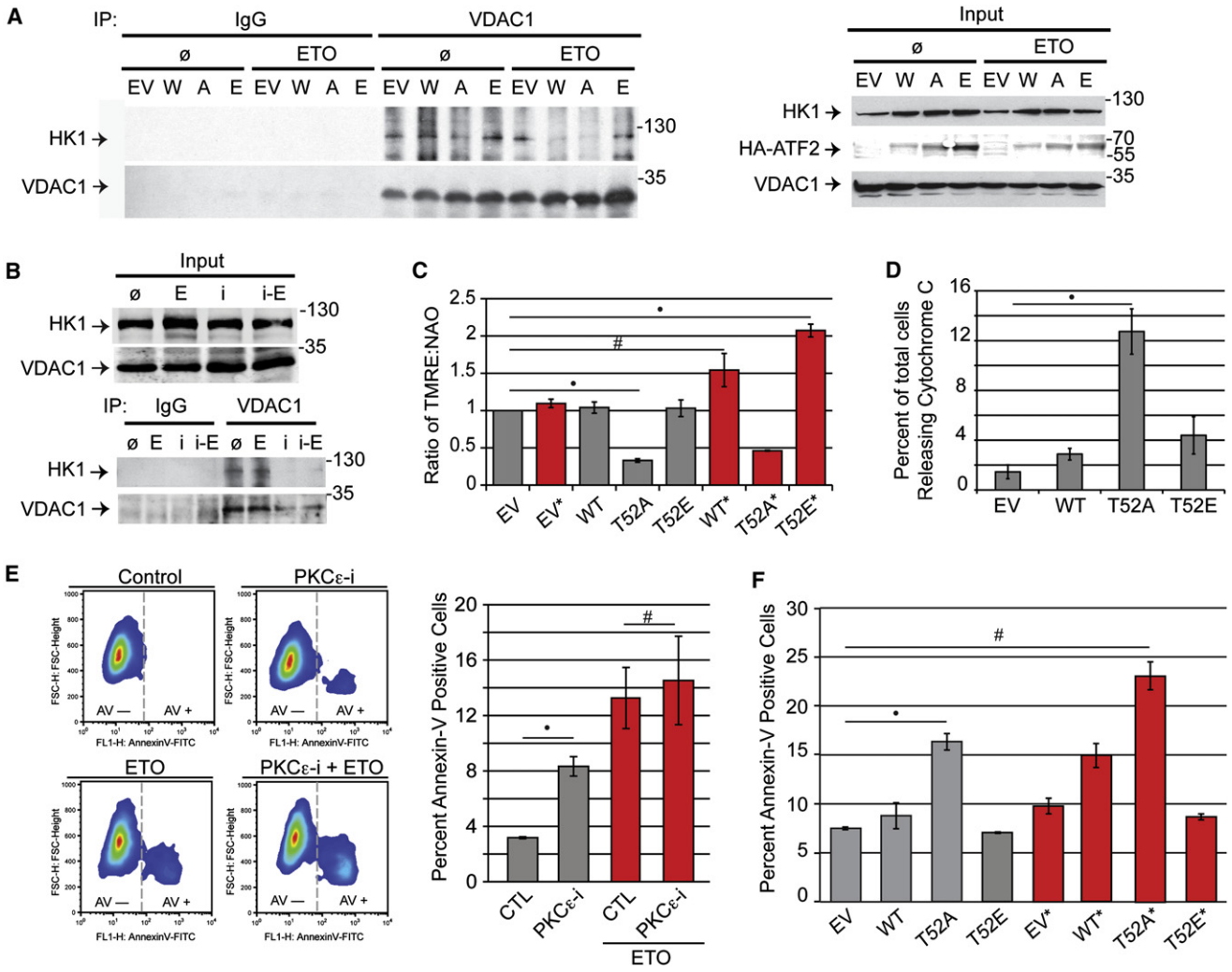

Figure 5. ATF2^{T52A} Abrogates HK1:VDAC Association, Promoting Mitochondrial Leakage, Cytochrome *C* Release, and Cell Death

(A) SCC9 cells were transfected with empty vector (EV) or HA-tagged ATF2 (W), ATF2^{T52A} (A), or ATF2^{T52E} (E) in the presence or absence of 5 μM etoposide (ETO, overnight), crosslinked and lysed for whole-cell lysate (input), or immunoprecipitated for VDAC1 and subject to immunoblot analysis with indicated antibodies.

(B) SCC9 cells were treated with ETO (E) or PKCε translocation inhibitor (i, 5 μM) or both (i-E), lysed for whole-cell lysate (input), or immunoprecipitated for VDAC1 and subject to immunoblot analysis with indicated antibodies.

(C) SCC9 cells transfected with EV, W, A, or E in the presence (red bars) or absence (gray bars) of 5 μM etoposide overnight were pulse labeled with tetramethylrhodamine ethyl ester (TMRE) or nonyl acridine orange (NaO) and were subsequently analyzed by FACS analysis. Histogram bars represent ratios of TMRE/NaO uptake. See Figure S4 for individual TMRE and NaO values. n = 10,000 cells per replicate; three replicates per condition were performed. •$p < 0.0001$; #$p = 0.01$.

(D) Coverslip-grown SCC9 cells transfected with EV, W, A, or E were immunostained for cytochrome *c* and MitoTracker and analyzed for cytochrome *c* release by fluorescence microscopy. n > 100 cells per replicate; three replicates per condition were performed. •$p = 0.0008$.

(E) (Right) SCC9 cells treated with PKCε-i (5 μM) alone or in the presence of ETO (overnight) were stained with Annexin-V and propidium iodide (PI) and were subject to FACS analysis. •$p < 0.0001$; #$p = 0.6018$. Representative FACS plots (left) and corresponding Annexin V-negative and Annexin V-positive (AV−, AV+) percentages are as follows: control (97%, 3%); PKCε-i (92%, 8%); ETO (89.5%, 11.5%); and ETO+PKCε-i (87%, 13%). Averaged value histograms (right) are displayed as indicated.

(F) SCC9 cells were transfected with EV, W, A, or E in the presence (red bars) or absence (gray bars) of ETO. Cells were stained with Annexin-V and were subject to FACS analysis. n = 10,000 cells per replicate; three replicates per condition were performed. •$p = 0.0001$; #$p < 0.0001$.

Error bars represent SD. See also Figures S4 and S5.

expression induced cytochrome *c* leakage (Figure 5D, S5D). Interestingly, the IHC pattern of cytochrome *c* release is reflective of partial leakage (Carvalho et al., 2004), suggesting that mitochondrial ATF2 serves as a priming/initial trigger for sensitization, which precedes cell death. That ATF2^{WT} expression did not decrease mitochondrial potential or induce cell death (Figure 5D) could be explained by its susceptibility to be phosphorylated on T52 and retained in the nucleus. Hence, partial

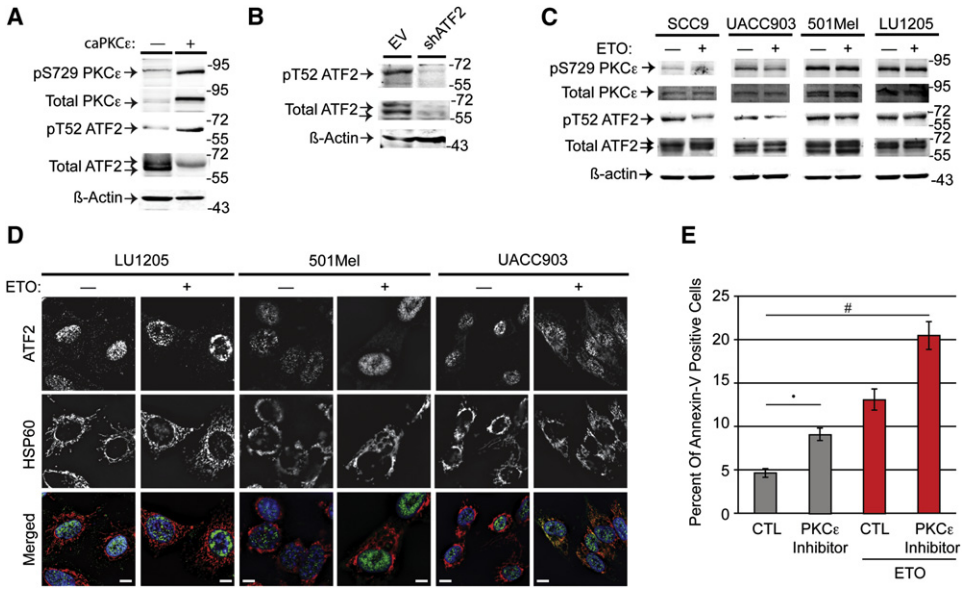

Figure 6. PKCε Phosphorylation of ATF2 on Thr52 and Resistance of Melanoma Cells to Genotoxic Stress-Induced Cell Death

(A) SCC9 cells were transfected with empty vector or constitutively active PKCε (caPKCε) and were subject to immunoblot analysis with indicated antibodies. Densitometric ratios of bands for (−caPKCε, +caPKCε) are as follows: pS729/β-actin (0.193, 0.636); pT52/Total ATF2 (0.215, 0.662).

(B) Control or ATF2 knocked down LU1205 cells were subject to immunoblot analysis with indicated antibodies.

(C) Indicated cell lines were subject to etoposide treatment (10 μM, ETO, overnight) and subject to immunoblot analysis with indicated antibodies. Densitometric band ratios for pT52/Total ATF2 (−ETO, +ETO) are as follows: SCC9 (1, 0.4), UACC903 (1, 0.7), 501Mel (1, 0.9), LU1205 (1, 1). Densitometric band ratios for pS729/Total PKCε (−ETO, +ETO) are as follows: SCC9 (1, 0.7), UACC903 (1, 0.7), 501Mel (1, 0.97), LU1205 (1, 1).

(D) Control or ETO-treated coverslip-grown LU1205, 501Mel, or UACC903 cells were immunofluorescently stained with indicated antibodies.

(E) 501Mel cells treated with 10 μM PKCε translocation inhibitor (PKCε-i) alone or in the presence or absence of 5 μM etoposide (ETO, overnight) were stained with Annexin-V and subject to FACS analysis. n = 10,000 cells per replicate; three replicates per condition were performed. •p = 0.0009; #p = 0.0001.

Error bars represent SD. See also Figure S6.

inhibition of PKCε is expected to allow partial nuclear retention of ATF2, whereas ATF2^{T52A} is largely excluded from the nuclei. Indeed, nuclear localization is seen in ~40% of the ATF2^{WT}-expressing cells (Figure S4D), which may dampen the effect elicited by the cytosolic ATF2. These observations suggest that a minimal level of ATF2 must reach the mitochondria in order to affect membrane potential and to promote cell death.

As mitochondrial leakage often precedes cell death, we evaluated whether mitochondria-localized ATF2 would sensitize cells to genotoxic stress-induced cell death. We examined how PKCε inhibition affected SCC9 cells exposed to genotoxic stress. Cells treated with PKCε-i exhibited increased Annexin-V labeling, similar to ETO-treated cells (Figure 5E). The latter is consistent with the observation that PKCε activation was equally attenuated upon ETO or PKCε-i treatment (Figure 3D). Furthermore, cells subjected to PKCε-i or siRNA-mediated knockdown of PKCε also exhibited increased cell death after ETO or UVC (20 J/m^2) treatment (Figures S5A and S5B). Consistently, expression of ATF2^{T52A}, but not ATF2^{WT} or ATF2^{T52E}, also resulted in elevated cell death, regardless of genotoxic stress (Figure 5F).

Given the importance of Bax in the permeabilization of mitochondria and control of cell death, we assessed possible changes in the conformation and thus activation of Bax. Using antibodies recognizing active conformation of Bax, we revealed that ATF2^{T52A} promotes active Bax conformation, whereas ATF2^{T52E} attenuates such conformation (Figure S5E).

PKCε Expression Increases T52 Phosphorylation of ATF2 and Melanoma Cells' Resistance to Genotoxic Stress

To monitor PKCε phosphorylation of ATF2 on T52, we generated a polyclonal antibody against phosphorylated T52 (pT52 antibody). caPKCε overexpression in SCC9 cells resulted in the appearance of a slower-migrating band that was recognized by total and pT52 ATF2 antibodies (Figure 6A). Both total ATF2 and pT52 ATF2 bands were no longer detectable upon ATF2 knockdown (Figure 6B).

We next evaluated the status of pT52 in SCC9 as well as melanoma cell lines prior to and after genotoxic stress. Consistent with reduced PKCε phosphorylation of ATF2 on T52, pT52 levels were lower in SCC9 cells subjected to ETO treatment (Figure 6C). Of note, whereas decreased T52 phosphorylation was also apparent in ETO-treated UACC903 cells, it was much less pronounced in 501Mel and LU1205 cells. These findings are consistent with the relationship between PKCε activity and the ability of ATF2 to translocate to the mitochondria following genotoxic stress. Respectively, UACC903 cells, but not LU1205 or 501Mel cells, exhibited partial mitochondrial translocation of ATF2 following ETO treatment (Figures 6C

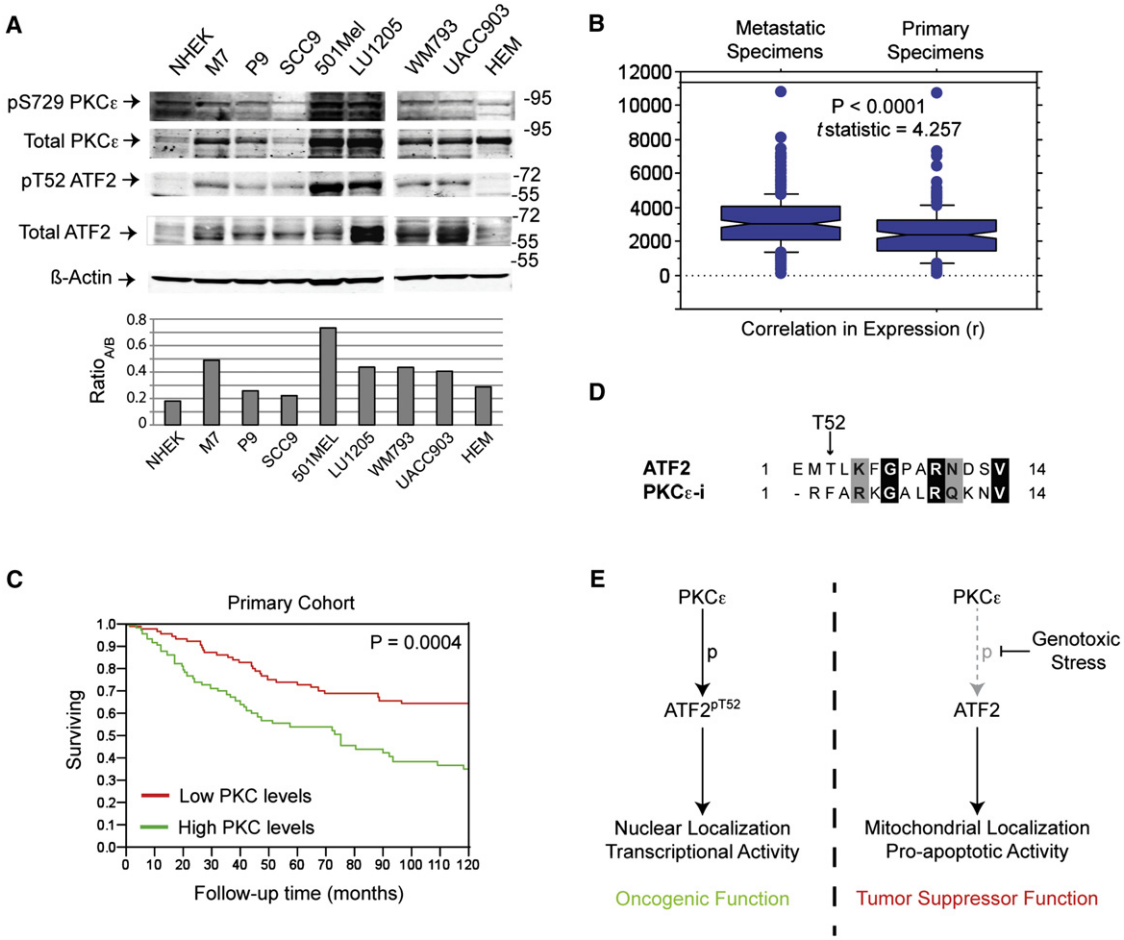

Figure 7. PKCε and Phospho-T52 ATF2 Expression in Normal Cells and Malignant Tumors

(A) Primary keratinocytes (NHEK) and melanocytes (HEM), squamous carcinoma (M7, P9, SCC9), and melanoma (501Mel, LU1205, WM793, and UACC903) cell lines were subject to immunoblot analysis with indicated antibodies. Histogram represents ratio A/B, where A = densitometric ratio values of pT52/total ATF2 bands and B = densitometric ratio values of pS729/total PKCε bands.

(B) Box plots showing distribution of PKCε in metastatic (left) and primary (right) specimens. PKCε levels are denoted on the y axis ($p < 0.0001$, t statistic –4.257). The mean ± one standard deviation is depicted by the horizontal bars and is higher in the metastatic specimens.

(C) Kaplan Meier survival curves showing significantly shorter survival in primary tumors expressing higher PKCε.

(D) Alignment of amino acid sequences flanking Thr52 in ATF2, as compared to consensus sequence used as PKCε inhibitor peptide.

(E) Schematic representation of PKCε-mediated regulation of the subcellular localization and, therefore, the oncogene or tumor suppressor activities of ATF2.

See also Figure S7.

and 6D). Correspondingly, LU1205 and 501Mel cells were more resistant to cell death compared with UACC903, SCC9, or P9 (an SCC line with low PKCε levels) (Figure S6A), further supporting the notion that melanoma resistance to genotoxic stress-induced cell death is due to impaired mitochondrial translocation of ATF2. Consistent with these observations and the nuclear localization of the $ATF2^{T52E}$ mutant, immunostaining with the pT52 antibody detected only nuclear ATF2 (Figure S7A). These findings suggest that elevated PKCε levels in melanoma cells inhibit ATF2 localization and function at the mitochondria, thereby attenuating its role in promoting cell death following genotoxic stress.

To establish the relationship between PKCε activity, pT52 phosphorylation, and sensitization to genotoxic stress-induced apoptosis, we manipulated PKCε or ATF2 in MEL501 and SCC9 cells. Whereas MEL501 cells exhibit high levels of PKCε, T52 phosphorylation, and impaired ATF2 translocation to the mitochondria (Figure 6C, 6D and 7A), SCC9 have low levels of PKCε, T52 phosphorylation, and ATF2 localization at the mitochondria following genotoxic stress (Figures 1, 6C, and 7A). ETO or UVC treatment, combined with PKCε-i or expression of PKCε-targeted siRNA, sensitized 501MEL to genotoxic stress-induced cell death (Figures 6E and S5C). Conversely, $ATF2^{T52E}$-expressing SCC9 cells exhibited lower levels of the early apoptotic marker Annexin-V in response to ETO, PKCε-i, or a combination of both, compared to EV- or $ATF2^{WT}$-expressing cells (Figure S6B), corroborating the prosurvival function associated with T52 phosphorylation. Intriguingly, although

stable EV, ATF2^{WT}, or ATF2^{T52E} expression in SCC9 cells produced no significant effects in proliferation rate during non-stressed conditions, ATF2^{T52E} conferred a survival advantage when the cells were grown in the presence of ETO (Figure S6C), further demonstrating the prosurvival effects conferred by pT52-ATF2.

High Expression of PKCε in Melanoma Tumors Is Associated with Poor Prognosis

To assess the nature of the differences in genotoxic stress resistance between melanoma and SCC cells, we surveyed the degree of PKCε expression and activity in a panel of melanoma cell lines and a large cohort of melanoma tissue arrays (TMA). Overall, melanoma cell lines exhibited higher PKCε expression than primary keratinocytes, melanocytes, or SCC lines (Figure 7A). Of note, pT52 was lowest in primary keratinocytes and melanocytes, whereas its levels were highest in 501Mel and LU1205, where total and pS729 (active) PKCε levels are the highest.

We next studied the association between PKCε expression levels, patient survival, and other clinical and pathological factors. IHC of a melanoma TMA revealed fairly homogenous cytoplasmic/membranous staining within each histospot (Figure S7B). Immunofluorescent intensity was measurable in 427 histospots (171 primary and 256 metastatic cases).

PKCε expression was higher in metastatic than primary specimens ($p < 0.0001$), as shown in Figure 7B. In primary specimens, PKCε levels were higher in thicker lesions ($p < 0.0001$) and in ulcerated lesions ($p = 0.0004$). PKCε expression did not correlate with age, gender, or presence of tumor-infiltrating lymphocytes.

Cox univariate survival analysis of continuous immunofluorescent intensity scores indicated that high PKCε expression was associated with decreased survival in the primary cohort ($p = 0.00042$), but not in the metastatic subset ($p = 0.887$). Multivariate analysis of PKCε expression did not retain its independent prognostic value, presumably due to the strong association with Breslow depth. To visually demonstrate the association between PKCε expression and survival, we dichotomized the continuous scores by the median score. High PKCε expression was not associated with survival in the metastatic subset of patients (log rank $p = 0.8$; Figure S7C) but, rather, was strongly associated with decreased survival in the primary cohort (log rank $p = 0.0004$; Figure 7C), consistent with our earlier analyses of a similar cohort in which nuclear localization of ATF2 correlated with poor prognosis (Berger et al., 2003).

Recent global mRNA expression profiling analyses (Yu et al., 2008) revealed that ATF2 and VDAC1 expression are highly correlated in nonmalignant tissue samples but significantly less correlated in basal cell carcinoma (Figures S7D and S7E). Independent expression profiling of metastatic versus nonmetastatic melanoma (Xu et al., 2008) also identified that ATF2 and VDAC1 expression are significantly more correlated in primary melanoma than in aggressive metastases (Figures S7F and S7G). These analyses are consistent with the ability to predict cancer outcome using dynamic modularity in protein interaction networks (Taylor et al., 2009).

DISCUSSION

A number of transcription factors, including Myc, Notch, and β-catenin, exhibit both oncogenic and tumor suppressor activities (Koch and Radtke, 2007; Larsson and Henriksson, 2010), yet the mechanism(s) controlling their opposing functions are largely associated with a given tissue/cell type. Here, we demonstrate that the tumor suppressor or oncogenic activities of ATF2 result from its cytosolic or nuclear function, respectively (Figure 7E). Cytosolic localization of ATF2 has been seen in nonmalignant skin tumors where ATF2 exhibits tumor suppressor activity. Thus, mice expressing a transcriptionally inactive form of ATF2 in keratinocytes developed more rapid and larger skin papillomas than wild-type mice when subjected to DMBA-TPA skin carcinogenesis (Bhoumik et al., 2008). In addition, p53 mutant mice lacking ATF2 in mammary tissues had a higher incidence of mammary tumors (Maekawa et al., 2008). In contrast to these tumor suppressor activities, ATF2 plays an oncogenic role in malignant melanoma. Inactivation of ATF2 in melanocytes attenuates melanoma formation in the mutant N-Ras/Ink4a model (Shah et al., 2010). Unlike in BCC/SCC, where ATF2 is also cytosolic, ATF2 is predominantly nuclear in melanoma, which is associated with poor prognosis (Berger et al., 2003).

The present findings reveal that, following genotoxic stress, cytosolic ATF2 impairs HK1/VDAC1 complexes and mitochondrial membrane integrity, sensitizing cells to apoptosis. In contrast, the high PKCε expression in melanoma cells induces predominantly nuclear localization of ATF2, which attenuates its normal cytosolic function and correlates with resistance to genotoxic stress. Of note, the different levels of PKCε activity found in melanomas determine the extent to which ATF2 reaches the mitochondria and promotes cell death following genotoxic stress. Thus, PKCε dictates the tumor suppressor or oncogenic activities of ATF2 by directly affecting its nuclear or cytosolic localization.

Though transcription factors such as p53, CREB, Stat3, and Elk-1 have been reported to localize at the mitochondria (Barrett et al., 2006; Lee et al., 2005; Mihara et al., 2003; Wegrzyn et al., 2009), the finding that ATF2 can switch between its oncogenic transcriptional function and its tumor suppressor mitochondrial function presents a new paradigm for transcription factor regulation and function. We show that the ability of ATF2 to abrogate the HK1/VDAC complex is perturbed in melanomas, which offers insight into the mechanisms underlying the notorious resistance of melanoma to therapy. Consistent with this, HK/VDAC1 complexes are increased in cancer cells and are associated with induction of the Warburg effect and a tumorigenic advantage (Mathupala et al., 2006). PKCε may play an indirect role in the metabolic changes that contribute to cancer development and/or progression, as suggested by the observation that elevated PKCε activity antagonizes the HK1/VDAC1-perturbing function of ATF2. Of note, Bax activation is induced by ATF2^{T52A} and reduced by ATF2^{T52E} (Figure S5E), which may be associated with the effect seen on HK1/VDAC or may be reflective of additional activities elicited by cytosolic/mitochondrial ATF2.

Multivariate analysis did not identify PKCε expression as an independent prognostic marker for melanoma, implying that it

may not be a driver of melanoma progression. This would be consistent with our finding that ATF2^{T52E} confers a survival advantage during genotoxic stress but does not confer a proliferative advantage (Figures S6B and S6C) or anchorage-independent growth (data not shown). The upregulation of PKCε seen in metastatic melanomas explains how ATF2 mitochondrial function is attenuated and why nuclear localization of ATF2 is associated with poor prognosis in melanoma. Although many cancers show a correlation between elevated PKCε expression/activity and poor prognosis and chemotherapeutic resistance, the ATF2 status in these tumors is unknown (Bae et al., 2007). Of note, efforts to target PKCε for cancer therapy have met with limited success, primarily because of its similarity to PKCδ (Gonelli et al., 2009). Small molecules that induce cytosolic localization of ATF2 may thus represent a new class of compounds with a unique advantage for therapy, and more specific PKCε inhibitors may also be effective in this capacity.

We previously identified 10 and 50 aa ATF2-derived peptides that inhibited the transcriptional activity and increased the cytosolic localization of ATF2 (Bhoumik et al., 2004). These peptides (which encompassed T52) sensitized melanoma cells to apoptosis and inhibited melanoma growth in syngeneic mice and in human melanoma xenografts (Bhoumik et al., 2002). Based on our current findings, we propose that these peptides competitively inhibited PKCε phosphorylation of endogenous ATF2, thereby enabling its cytosolic localization and mitochondrial function. Consistent with this, mutation of T52 within the peptides abolished their inhibitory effects (Bhoumik et al., 2004). Strikingly, the amino acid sequences flanking T52 showed marked similarities to known PKC peptide inhibitors and satisfied the requirements for optimal PKC substrate sequence (Nishikawa et al., 1997). Though most PKC isoenzymes strongly prefer peptides with basic amino acids at the −2 position, PKCε also accepts glutamic acid, which is the residue found at this position in the ATF2 peptide (Figure 7D).

Our findings suggest a need to re-evaluate the functional significance of T52 phosphorylation by PKCε to ATF2 transcriptional activity and the relationship to phosphorylation on Thr69/71 by JNK/p38. We showed that caPKCε induces ~25-fold increase in Jun2-promoter activity, compared to only ~6-fold increased activity induced by ATF2^{T52E} (Figures 3G and 3H), suggesting that PKCε may augment ATF2 phosphorylation by JNK, p38, or other PKC isoforms (Yamasaki et al., 2009). T52 phosphorylation of ATF2 may also affect the transcriptional function of ATF2 or its heterodimerization partners (Liu et al., 2006) and/or the role of ATF2 in the DNA damage response, which requires its phosphorylation on S490/498 by ATM (Bhoumik et al., 2005).

Collectively, our results establish the role of ATF2 at the mitochondria following genotoxic stress and reveal its contribution to stress-induced cell death. The degree of PKCε phosphorylation of ATF2 is instrumental in controlling its function. PKCε phosphorylation determines the ability of ATF2 to function at the mitochondria, where its contribution to cell death is consistent with its tumor suppressor functions. Constitutively high PKCε expression/activity, as seen in melanomas, attenuates ATF2 mitochondrial function and enhances its nuclear transcriptional activity, consistent with its oncogenic activity. Thus, PKCε regulates the subcellular localization of ATF2, which dictates its ability to elicit oncogenic or tumor suppressor activities.

EXPERIMENTAL PROCEDURES

Cell Lines

Squamous cell carcinoma (SCC9) cells were maintained in Dulbecco's modified Eagle's medium (DMEM):F-12 (50:50) (Hyclone/Thermo Scientific, USA) supplemented with 400 ng/ml hydrocortisone, 10% fetal bovine serum (FBS), and antibiotics. Melanoma cell lines, M7, P9, and human skin fibroblasts were maintained in Dulbecco's modified Eagle's medium (DMEM) supplemented with 10% FBS and antibiotics. Normal human epidermal keratinocytes (NHEK) cells were maintained in KGM-2 growth medium (Lonza, USA). Melanocytes were maintained in 254 Medium (Invitrogen, CA, USA).

Antibodies and Immunostaining Reagents

Antibodies employed were purchased as follows: ATF2 (20F1), HK1 (C35C4), HK2 (C64G5), HA (C29F4, for immunoblot analysis), and COXIV (3E11) from Cell Signaling Technologies (MA, USA); β-actin (9), HIS-probe (H-15), HSP90 (4F10), Lamin A (N-16), PKCε (C15), TOM20 (F-10), and VDAC1 (20B12) from Santa Cruz Biotechnology, Inc. (CA, USA); HA (3F10, for immunofluorescent staining) from Roche; COXI (21C11BC11), COXII (2E3), COX IV (20E8), and pS729 PKCε (44977G) from Invitrogen (CA, USA); HSP60 (24) from BD PharMingen (USA); pT52 ATF2 from PhosphoSolutions (CO, USA); and Bax (6A7) from ExAlpha Biologicals (MA, USA). MitoTracker Red CMXRos, PKCε translocation inhibitor, Gö6850, and Leptomycin B were purchased from Invitrogen (CA, USA), Santa Cruz Biotechnologies, (CA, USA), EMD Chemicals (NJ, USA), and Sigma (USA), respectively.

Immunocytochemical Analysis

After indicated treatments, coverslip-grown cells were fixed in fixation buffer for 20 min at room temperature. Coverslips were then rinsed twice in phosphate buffer solution and permeabilized in permeabilization buffer for 20 min. Primary antibodies were applied at 1:250 dilution in staining buffer overnight at 4°C in a humid chamber. Coverslips were subsequently subject to five standing 5 min washes in wash buffer. Secondary antibodies (Alexa Fluor secondary 350, 488, or 568; Invitrogen) were applied at 1:250 dilution in staining buffer for 2–3 hr at room temperature in a humid chamber in the dark. Prior to mounting with Vectorshield with DAPI (Vector Laboratories, CA), coverslips were washed twice more in wash buffer. Immunofluorescent analysis was conducted on an Olympus TH4-100 fluorescent microscope. ≥ 3 Z planes per field were captured and analyzed using Slidebook V.4.1, and Z projection images of average intensity were constructed using ImageJ V.1.43u.

Analysis of ATF2 Transcriptional Activity

SCC9 cells were stably knocked down for ATF2 employing shRNA targeted for ATF2 3′UTR (ID: TRCN0000013713, Sigma, USA). In brief, lentiviral particles packaged with ATF2 3′UTR shRNA or pLKO empty vector constructs were generated and spin infected in the presence of 10 μg/ml polybrene (Sigma, USA) onto SCC9 cells. After 14 hr of infection, media was changed and cells were grown for an additional 8 hr before a second spin infection. Media was changed subsequently, and cells were grown for an additional 3 days in the presence of 0.8 μg/ml puromycin (Sigma, USA). Knocked down cells were plated in 96-well plates (3,000 cells/well). Each well was transfected with 6 ng pCMV β-galactosidase, 12 ng pGL-Jun2-promoter construct, and 30 ng of empty vector or pEF-HA-ATF2 (WT, T52A, or T52E mutants) overnight using JetPrime (Polyplus, France). Luciferase activity was evaluated using the Luciferase Assay System (Promega, WI) and was normalized by standardized β-gal assay.

Measurement of Mitochondrial Membrane Potential and Mass

After treatment as indicated in the figure legend, cells were pulse labeled with either 250 nM tetramethylrhodamine ethyl ester (TMRE; Invitrogen, CA, USA) or 10 nM nonyl acridine orange (NaO; Invitrogen, CA) (in PBS) for 20 min at

37°C to measure either membrane potential or mass, respectively. TMRE is a cationic dye preferentially taken up by mitochondria and generally reflects changes in overall mitochondrial membrane potential. NaO is a cardiolipin-specific (mitochondrial-specific lipid) staining dye that is reflective of mitochondrial mass, which is generally unchanged during acute membrane potential changes (King et al., 2007). After labeling, cells were harvested by trypsinization and resuspended in 150 nM TMRE or 5 nM NaO, respectively, and analyzed immediately by fluorescence-activated cell sorting (FACS). n = 10,000 cells (within whole-cell gates) per replica in over three independent experiments. FACS data were subsequently analyzed by FlowJo software (TreeStar, OR, USA).

Immunoprecipitation of VDAC1:HK1:ATF2 Complexes

After indicated treatments, cells were washed once with PBS at room temperature and crosslinked with 1 mM dimethyl 3,3′-dithiopropionimidate dihydrochloride (DTBP; Sigma, USA) in PBS. Cells were harvested and pelleted, washed five times with PBS, and resuspended in lysis buffer for 20 min on ice (1% Triton X-100/0.05% CHAPS/20 mM Tris [pH 7.5]/150 mM NaCl/1 mM EDTA/1 mM EGTA/protease and phosphatase inhibitors). Cell lysates were sonicated with a microtip sonicator (Fisher Scientific Sonic Dismembrator, Model 100) for 5 s (setting 1:~4 W output) on ice and pelleted, and resulting supernatant was reserved. Pellets were resuspended in new lysis buffer and sonicated again for 15 s (setting 2:~6 W output) on ice. Twice-sonicated lysates were pelleted, and supernatants were combined and subjected to immunoprecipitation overnight with indicated antibodies.

DNA Construct sh/siRNAs and Transfection Methods

DNA plasmids were all transfected using JetPrime according to manufacturer's protocol (Polyplus, France). Lentiviral vector against PKCζ and constitutively active HIS-tagged PKCε were generous gifts from Dr. Jorge Moscat. siRNA was transfected using RNAiMax according to manufacturer's protocol (Invitrogen, CA). All siRNAs were obtained from Ambion (USA): siHK1-1 (ID: 1599); siHK1-2 (1689); siHK2-1 (ID: 1433); siPKCε (ID: 677); and siPKCδ (ID: 775).

Tumor Microarray Analysis

Melanoma tissue microarrays have been previously described and were processed as in Qi et al. (2010) with minor modifications for immunofluorescent staining. PKCε antibody was applied at 1:300 dilution, and Alexa Fluor 488 secondary (Invitrogen) was applied at 1:400 dilution. The TMA was counterstained with 4′,6-diamidino-2-phenylindole (DAPI). Images were captured by fluorescence microscopic scanning, employing Aperio ScanScope. Integrated signal intensity from all individual histospots was measured by two independent scorers in blind manner, using ImageJ software. With the assistance of a secondary blinded scorer, tumor spots were classified as uninterpretable if they had insufficient tumor cells, loss of tissue, or abundant necrosis based on DAPI counter staining. PKCε intensity scores ranged from 87 to 10,838 (median: 2764), and data were analyzed by a third evaluator.

SUPPLEMENTAL INFORMATION

Supplemental Information includes Extended Experimental Procedures, seven figures, and one table and can be found with this article online at doi:10.1016/j.cell.2012.01.016.

ACKNOWLEDGMENTS

We thank Meenhard Herlyn and John Clifford for melanoma and SCC cell lines, Jorge Moscat and Maria Diaz-Meco for PKC reagents, members of the Salvesen lab, Robbin Newlin and Yoav Altman for technical assistance, and Colin Goding for helpful comments on the manuscript. We also thank Ronai laboratory members, Meifan Chen, Hyungsoo Kim, Ersheng Kuang, Marzia Scortegagna, and Meera Shah for technical advice and assistance and Gustavo Gutierrez for bacterial ATF2 proteins. Support from ACS Postdoctoral Fellowship, Illinois Division and NCI T32 training grant (117090-PF-09-112-01-GMC and 5-T32-CA121949 to E.L.) and NCI grants (CA099961 and CA051995 to Z.A.R.) are gratefully acknowledged. D.L.R. is a consultant for and stockholder in HistoRx, the exclusive licensee of the Yale-owned AQUA technology used in this work.

Received: February 6, 2011
Revised: August 12, 2011
Accepted: January 6, 2012
Published: February 2, 2012

REFERENCES

Abu-Hamad, S., Arbel, N., Calo, D., Arzoine, L., Israelson, A., Keinan, N., Ben-Romano, R., Friedman, O., and Shoshan-Barmatz, V. (2009). The VDAC1 N-terminus is essential both for apoptosis and the protective effect of anti-apoptotic proteins. J. Cell Sci. *122*, 1906–1916.

Bae, K.M., Wang, H., Jiang, G., Chen, M.G., Lu, L., and Xiao, L. (2007). Protein kinase C epsilon is overexpressed in primary human non-small cell lung cancers and functionally required for proliferation of non-small cell lung cancer cells in a p21/Cip1-dependent manner. Cancer Res. *67*, 6053–6063.

Barrett, L.E., Van Bockstaele, E.J., Sul, J.Y., Takano, H., Haydon, P.G., and Eberwine, J.H. (2006). Elk-1 associates with the mitochondrial permeability transition pore complex in neurons. Proc. Natl. Acad. Sci. USA *103*, 5155–5160.

Berger, A.J., Kluger, H.M., Li, N., Kielhorn, E., Halaban, R., Ronai, Z., and Rimm, D.L. (2003). Subcellular localization of activating transcription factor 2 in melanoma specimens predicts patient survival. Cancer Res. *63*, 8103–8107.

Bhoumik, A., Fichtman, B., Derossi, C., Breitwieser, W., Kluger, H.M., Davis, S., Subtil, A., Meltzer, P., Krajewski, S., Jones, N., and Ronai, Z. (2008). Suppressor role of activating transcription factor 2 (ATF2) in skin cancer. Proc. Natl. Acad. Sci. USA *105*, 1674–1679.

Bhoumik, A., Huang, T.G., Ivanov, V., Gangi, L., Qiao, R.F., Woo, S.L., Chen, S.H., and Ronai, Z. (2002). An ATF2-derived peptide sensitizes melanomas to apoptosis and inhibits their growth and metastasis. J. Clin. Invest. *110*, 643–650.

Bhoumik, A., Jones, N., and Ronai, Z. (2004). Transcriptional switch by activating transcription factor 2-derived peptide sensitizes melanoma cells to apoptosis and inhibits their tumorigenicity. Proc. Natl. Acad. Sci. USA *101*, 4222–4227.

Bhoumik, A., Takahashi, S., Breitweiser, W., Shiloh, Y., Jones, N., and Ronai, Z. (2005). ATM-dependent phosphorylation of ATF2 is required for the DNA damage response. Mol. Cell *18*, 577–587.

Carvalho, A.C., Sharpe, J., Rosenstock, T.R., Teles, A.F., Youle, R.J., and Smaili, S.S. (2004). Bax affects intracellular Ca2+ stores and induces Ca2+ wave propagation. Cell Death Differ. *11*, 1265–1276.

Deng, X., Liu, H., Huang, J., Cheng, L., Keller, E.T., Parsons, S.J., and Hu, C.D. (2008). Ionizing radiation induces prostate cancer neuroendocrine differentiation through interplay of CREB and ATF2: implications for disease progression. Cancer Res. *68*, 9663–9670.

Fu, X., Wan, S., Lyu, Y.L., Liu, L.F., and Qi, H. (2008). Etoposide induces ATM-dependent mitochondrial biogenesis through AMPK activation. PLoS One *3*, e2009.

Gillespie, S., Zhang, X.D., and Hersey, P. (2005). Variable expression of protein kinase C epsilon in human melanoma cells regulates sensitivity to TRAIL-induced apoptosis. Mol. Cancer Ther. *4*, 668–676.

Gonelli, A., Mischiati, C., Guerrini, R., Voltan, R., Salvadori, S., and Zauli, G. (2009). Perspectives of protein kinase C (PKC) inhibitors as anti-cancer agents. Mini Rev. Med. Chem. *9*, 498–509.

Gupta, S., Campbell, D., Dérijard, B., and Davis, R.J. (1995). Transcription factor ATF2 regulation by the JNK signal transduction pathway. Science *267*, 389–393.

King, M.A., Eddaoudi, A., and Davies, D.C. (2007). A comparison of three flow cytometry methods for evaluating mitochondrial damage during staurosporine-induced apoptosis in Jurkat cells. Cytometry A *71*, 668–674.

Koch, U., and Radtke, F. (2007). Notch and cancer: a double-edged sword. Cell. Mol. Life Sci. *64*, 2746–2762.

Larsson, L.G., and Henriksson, M.A. (2010). The Yin and Yang functions of the Myc oncoprotein in cancer development and as targets for therapy. Exp. Cell Res. *316*, 1429–1437.

Lee, J., Kim, C.H., Simon, D.K., Aminova, L.R., Andreyev, A.Y., Kushnareva, Y.E., Murphy, A.N., Lonze, B.E., Kim, K.S., Ginty, D.D., et al. (2005). Mitochondrial cyclic AMP response element-binding protein (CREB) mediates mitochondrial gene expression and neuronal survival. J. Biol. Chem. *280*, 40398–40401.

Li, S., Ezhevsky, S., Dewing, A., Cato, M.H., Scortegagna, M., Bhoumik, A., Breitwieser, W., Braddock, D., Eroshkin, A., Qi, J., et al. (2010). Radiation Sensitivity and Tumor Susceptibility in ATM Phospho-Mutant ATF2 Mice. Genes Cancer *1*, 316–330.

Liu, H., Deng, X., Shyu, Y.J., Li, J.J., Taparowsky, E.J., and Hu, C.D. (2006). Mutual regulation of c-Jun and ATF2 by transcriptional activation and subcellular localization. EMBO J. *25*, 1058–1069.

Lopez-Bergami, P., Lau, E., and Ronai, Z. (2010). Emerging roles of ATF2 and the dynamic AP1 network in cancer. Nat. Rev. Cancer *10*, 65–76.

Maekawa, T., Sano, Y., Shinagawa, T., Rahman, Z., Sakuma, T., Nomura, S., Licht, J.D., and Ishii, S. (2008). ATF-2 controls transcription of Maspin and GADD45 alpha genes independently from p53 to suppress mammary tumors. Oncogene *27*, 1045–1054.

Mathupala, S.P., Ko, Y.H., and Pedersen, P.L. (2006). Hexokinase II: cancer's double-edged sword acting as both facilitator and gatekeeper of malignancy when bound to mitochondria. Oncogene *25*, 4777–4786.

Mihara, M., Erster, S., Zaika, A., Petrenko, O., Chittenden, T., Pancoska, P., and Moll, U.M. (2003). p53 has a direct apoptogenic role at the mitochondria. Mol. Cell *11*, 577–590.

Moin, S.M., Panteva, M., and Jameel, S. (2007). The hepatitis E virus Orf3 protein protects cells from mitochondrial depolarization and death. J. Biol. Chem. *282*, 21124–21133.

Nishikawa, K., Toker, A., Johannes, F.J., Songyang, Z., and Cantley, L.C. (1997). Determination of the specific substrate sequence motifs of protein kinase C isozymes. J. Biol. Chem. *272*, 952–960.

Pass, J.M., Zheng, Y., Wead, W.B., Zhang, J., Li, R.C., Bolli, R., and Ping, P. (2001). PKCepsilon activation induces dichotomous cardiac phenotypes and modulates PKCepsilon-RACK interactions and RACK expression. Am. J. Physiol. Heart Circ. Physiol. *280*, H946–H955.

Qi, J., Nakayama, K., Cardiff, R.D., Borowsky, A.D., Kaul, K., Williams, R., Krajewski, S., Mercola, D., Carpenter, P.M., Bowtell, D., and Ronai, Z.A. (2010). Siah2-dependent concerted activity of HIF and FoxA2 regulates formation of neuroendocrine phenotype and neuroendocrine prostate tumors. Cancer Cell *18*, 23–38.

Sand, J.M., Aziz, M.H., Dreckschmidt, N.E., Havighurst, T.C., Kim, K., Oberley, T.D., and Verma, A.K. (2010). PKCepsilon overexpression, irrespective of genetic background, sensitizes skin to UVR-induced development of squamous-cell carcinomas. J. Invest. Dermatol. *130*, 270–277.

Shah, M., Bhoumik, A., Goel, V., Dewing, A., Breitwieser, W., Kluger, H., Krajewski, S., Krajewska, M., Dehart, J., Lau, E., et al. (2010). A role for ATF2 in regulating MITF and melanoma development. PLoS Genet. *6*, e1001258.

Shoshan-Barmatz, V., Keinan, N., Abu-Hamad, S., Tyomkin, D., and Aram, L. (2010). Apoptosis is regulated by the VDAC1 N-terminal region and by VDAC oligomerization: release of cytochrome c, AIF and Smac/Diablo. Biochim. Biophys. Acta *1797*, 1281–1291.

Shulga, N., Wilson-Smith, R., and Pastorino, J.G. (2009). Hexokinase II detachment from the mitochondria potentiates cisplatin induced cytotoxicity through a caspase-2 dependent mechanism. Cell Cycle *8*, 3355–3364.

Taylor, I.W., Linding, R., Warde-Farley, D., Liu, Y., Pesquita, C., Faria, D., Bull, S., Pawson, T., Morris, Q., and Wrana, J.L. (2009). Dynamic modularity in protein interaction networks predicts breast cancer outcome. Nat. Biotechnol. *27*, 199–204.

van Dam, H., Wilhelm, D., Herr, I., Steffen, A., Herrlich, P., and Angel, P. (1995). ATF-2 is preferentially activated by stress-activated protein kinases to mediate c-jun induction in response to genotoxic agents. EMBO J. *14*, 1798–1811.

Wegrzyn, J., Potla, R., Chwae, Y.J., Sepuri, N.B., Zhang, Q., Koeck, T., Derecka, M., Szczepanek, K., Szelag, M., Gornicka, A., et al. (2009). Function of mitochondrial Stat3 in cellular respiration. Science *323*, 793–797.

Xu, L., Shen, S.S., Hoshida, Y., Subramanian, A., Ross, K., Brunet, J.P., Wagner, S.N., Ramaswamy, S., Mesirov, J.P., and Hynes, R.O. (2008). Gene expression changes in an animal melanoma model correlate with aggressiveness of human melanoma metastases. Mol. Cancer Res. *6*, 760–769.

Yamasaki, T., Takahashi, A., Pan, J., Yamaguchi, N., and Yokoyama, K.K. (2009). Phosphorylation of Activation Transcription Factor-2 at Serine 121 by Protein Kinase C Controls c-Jun-mediated Activation of Transcription. J. Biol. Chem. *284*, 8567–8581.

Yu, M., Zloty, D., Cowan, B., Shapiro, J., Haegert, A., Bell, R.H., Warshawski, L., Carr, N., and McElwee, K.J. (2008). Superficial, nodular, and morpheiform basal-cell carcinomas exhibit distinct gene expression profiles. J. Invest. Dermatol. *128*, 1797–1805.

Zalk, R., Israelson, A., Garty, E.S., Azoulay-Zohar, H., and Shoshan-Barmatz, V. (2005). Oligomeric states of the voltage-dependent anion channel and cytochrome c release from mitochondria. Biochem. J. *386*, 73–83.